Electronic supplementary information for

Covalent and non-covalent coupling of a Au_{102} nanocluster with a fluorophore: energy transfer, quenching and intracellular pH sensing.

Eero Hulkko,[#] Tanja Lahtinen,[#] Varpu Marjomäki,[£] Emmi Pohjolainen,[$] Ville Saarnio,[#] Karolina Sokolowska,[#] Ardra Ajitha,[#] Mikael Kuisma,[#] Lauri Lehtovaara,[#] Gerrit Groenhof,[#] Hannu Häkkinen,[#,$] Mika Pettersson[#]*

[#]Department of Chemistry, Nanoscience Center, P.O. Box 35, FI-40014, University of Jyväskylä, Finland.

[£]Department of Biology and Environmental Science, Nanoscience Center, P.O. Box 35, FI-40014, University of Jyväskylä, Finland.

[$]Department of Physics, Nanoscience Center, P.O. Box 35, FI-40014, University of Jyväskylä, Finland.

E-mail: mika.j.pettersson@jyu.fi

SI1. Additional details of pH-dependent spectroscopic measurements. Au_{102} and KU concentrations were determined using absorption coefficients ε_{541} = 9840 $cm^{-1}M^{-1}$ for KU-dye from Ref. [1], and ε_{600} = $15.4 \cdot 10^4$ $cm^{-1}M^{-1}$ for Au_{102} From Ref. [2]. The sample pH was determined using Mettler Toledo (MT) SevenEasy™ S20 pH-meter equipped with MT InLab@ microelectrode. The pH-meter was 3-point calibrated prior to the experiments using pH = 4.0,7.0, and 10.0 standard buffer-solutions (MT). Sample pH was adjusted by carefully adding µl amounts of dilute NaOH (basic) or HCl (acidic) to the sample solution, while simultaneously monitoring the acidity using the pH-meter. For the titration of non-covalently bound Au_{102}-KU with NaCl or PBS salt solutions, 1 µM stock solutions of Au_{102} and KU-orange were prepared in deionized water at pH 9. From the 1 µM stocks, solutions of Au_{102}-KU mixtures in 1:1 ratio at concentrations 0.5 µM, 0.25 µM and 0.125 µM were prepared, diluted to 2 ml final volume with deionized water (pH 9) if necessary. Aliquots (0 to 500 µl) of 1M NaCl or 25 x PBS solutions were added to the Au_{102}-KU solution and fluorescence spectra were collected between additions.

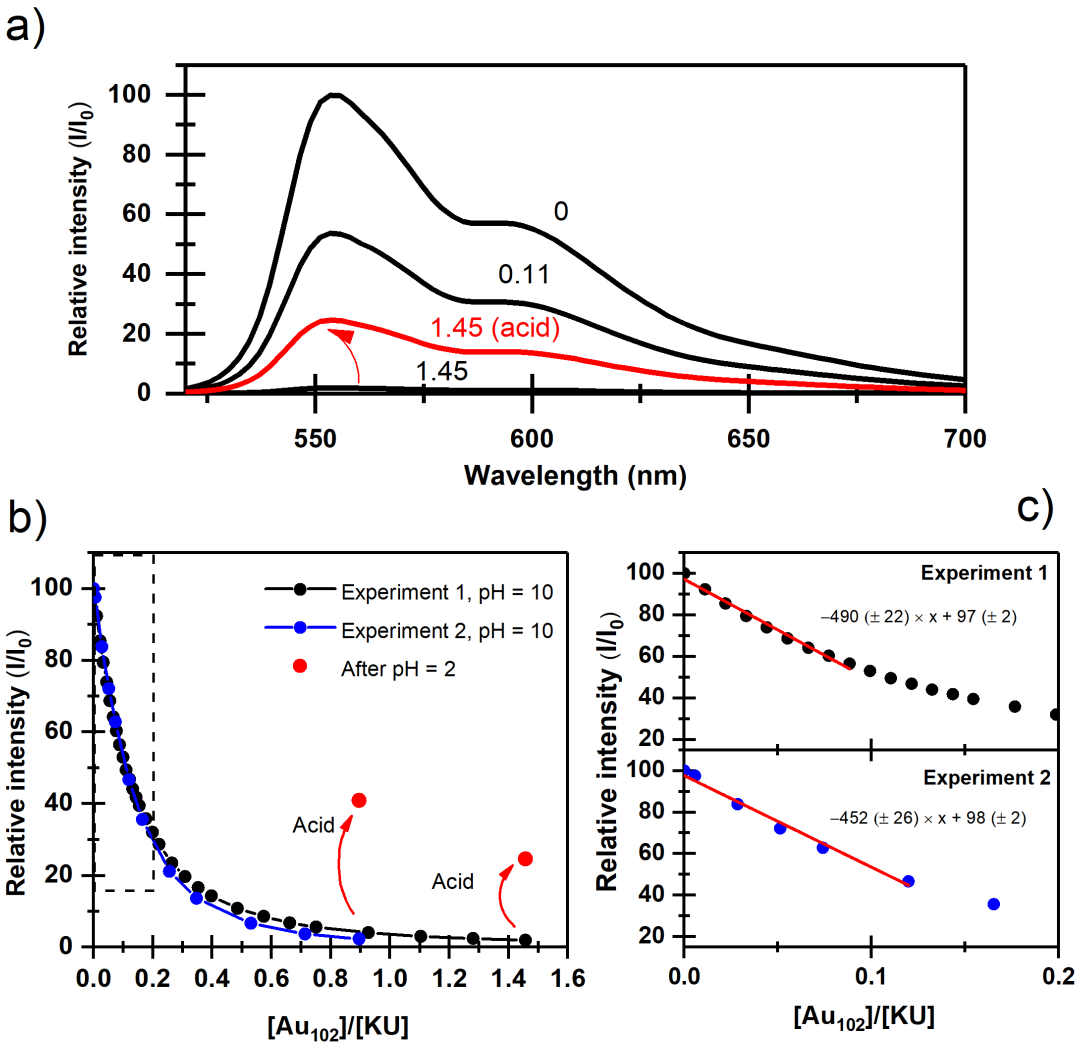

Figure SI2. **a)** Relative intensity of KU emission spectra with λ_{ex} = 500 nm excitation shown for selected [Au_{102}]/[KU] concentration ratios (ratios indicated in the figure) in basic conditions (pH = 10, black spectra). The maxima of the emission spectra at λ = 553 nm are normalized to 100 with the intensity of pure KU emission (I_0). The red spectrum shows the increase of the intensity after acidification of the solution (pH = 2, red spectrum). **b)** Normalized emission intensities of two Au_{102} titration experiments. Black points ($[Au_{102}]_{final}$ = 0.29 μM) and Blue points ($[Au_{102}]_{final}$ = 0.16 μM). Red points are intensities after acidification of the solution with HCl. **c)** Pseudo-linear intensity behaviour of KU fluorescence with small Au_{102} additions (dashed box in panel **b)**). Red lines are linear fits ($A+Bx$) to the intensity points, where the fitting parameters are shown in the panels (with fitting errors in the parenthesis). We estimated the approximate number of interacting KU molecules with one Au_{102} cluster from B/A ratio.

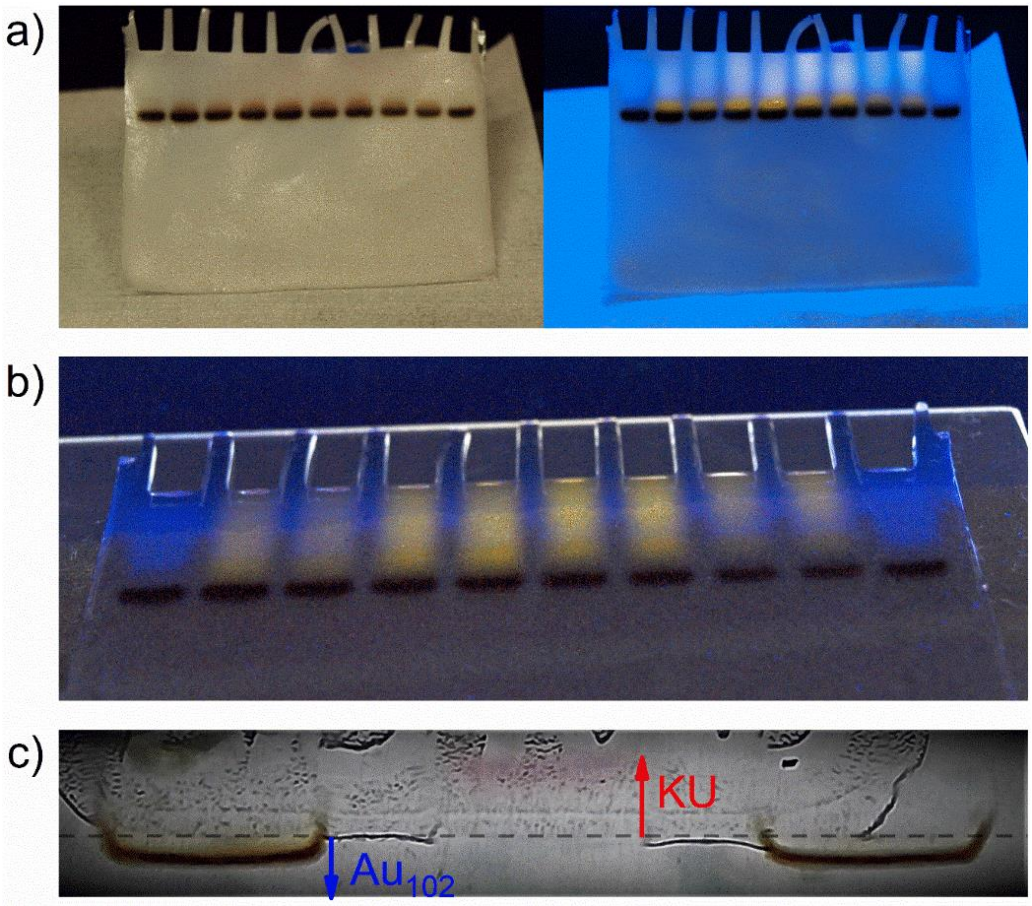

Figure SI3. a) Raw images of PAGE gels dried overnight in methanol (left) image taken in ambient light (right) image taken under UV-lamp (λ = 254). **b)** Image of the same PAGE gel under UV-light prior to drying in methanol. Note how the complex positions are not fluorescent before the drying. **c)** PAGE run of Au_{102} and water solution of KU. The gel level is indicated in the image with dashed line. Au_{102} is moving in the gel direction of blue arrow as the KU solution is moving in the opposite direction without any PAGE gel (red arrow). Image is taken under 130 V driving voltage in the beginning of the PAGE run. Image saturation and gamma-correction has been adjusted to make the KU band visible in the image.

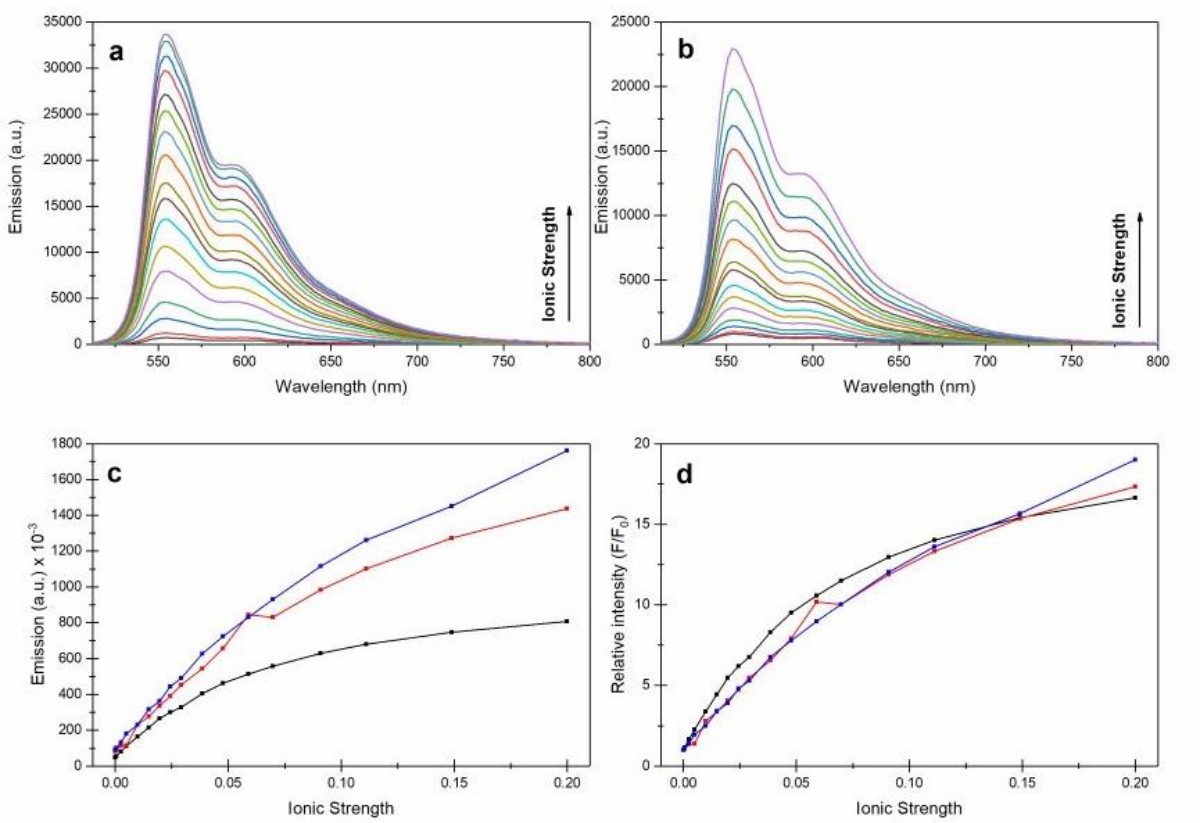

Figure SI4. a) Raw fluorescence spectra for the 0.5 µM sample titrated with 25x PBS showing the increase of emission intensity over the course of titration. **b)** Raw fluorescence spectra for the 0.5 µM sample titrated with 1 M NaCl showing the increase of emission intensity over the course of titration. **c)** Integrated emission intensity values and **d)** relative intensity of emission to the initial fluorescence of different Au_{102}-KU mixtures plotted with increasing ionic strength. Ionic strength was increased by adding aliquots of 1 M NaCl in room temperature. Concentration of Au_{102}-KU was 0.125 µM (black), 0.25 µM (red) and 0.5 µM (blue).

SI5 Molecular dynamics simulations

The simulations with covalently and non-covalently bound dye were performed in dodecahedric and cubic simulation boxes with periodic boundary conditions, respectively. We used TIP3P water model and a neutralizing concentration of NaCl as solvent in all simulations. We used the leapfrog integrator with a 2 fs time step, a 1.0 nm Lennard−Jones cutoff with dispersion correction for energy and pressure, PME (PME =particle mesh Ewald method) electrostatics with a 1.0 nm cutoff and 0.12 nm grid spacing, a velocity-rescale thermostat with a reference temperature of 300 K and a coupling time constant of 0.1 ps and the Berendsen barostat with a reference pressure of 1 bar and coupling time constant of 1 ps. All covalent bond lengths were constrained with the LINCS algorithm. Prior to the NPT production simulations, (250 ns and 100 ns for the systems with covalently and non-covalently bound dye, respectively) equilibrations of 100 ps NVT at 300 K + 1 ns NPT at 300 K, 1 bar and 1 fs time step were performed.

Molecular dynamics simulations of weakly bound complex. Molecular dynamics simulations were performed on the Au_{102}-KU complex to obtain an atomistic view on the interactions between the KU and the Au_{102} nanocluster. The simulations were performed with all pMBA groups of the nanocluster protonated (charge 0 e) or deprotonated (charge -44 e) to investigate the effects of the low and high pH, respectively. 100 ns simulations were performed with KU initially detached from the gold nanocluster. In both cases, with the fully protonated and fully deprotonated gold nanocluster, KU comes to close interaction with the nanocluster, and remains stable at the close distance during the remaining timescale of the simulation. The average structures of the last 10 ns of the simulations are presented in figure SI4.1. The average / standard deviation of the distance between KU and cluster center of mass for the last 10 ns of the simulation were 1.30 / 0.04 nm for the fully protonated and 1.29 / 0.03 nm for the fully deprotonated case, respectively.

The KU molecule adopts a similar, flat lying bonding orientation, independent of the cluster protonation state. More detailed look into distances between centers of mass of the KU and the pMBA groups shows that KU lies on average closer to the adjacent pMBA in the case of fully protonated cluster, compared to the fully deprotonated case.

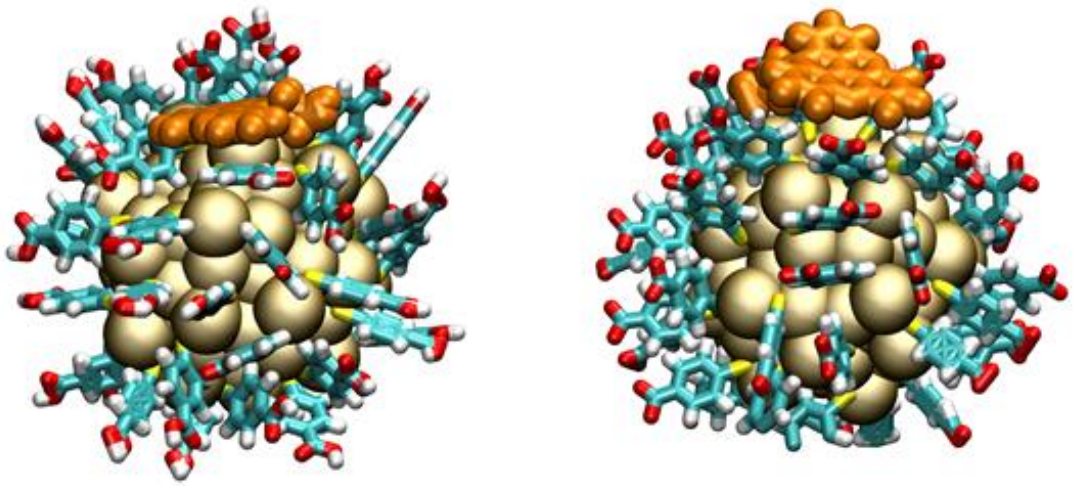

Figure SI5.1. Average structures from MD simulations of the fully protonated (left) and fully deprotonated (right) Au_{102} with non-covalently bound KU-dye.

Molecular dynamics simulations of the covalently bound hybrid. For the covalently attached KU we performed 250 ns simulations. Visual investigation revealed differences in the dye orientation and dynamics dependent on the protonation state of the cluster. The average structures are presented in figure SI4.2. Two distinct dye orientations with respect to the gold nanocluster can be distinguished. At the low pH (fully protonated cluster), the dye adopts a flat lying orientation with the average / standard deviation of distance between KU and cluster centers of mass of 1.34 / 0.03 nm. At high pH (fully deprotonated cluster), the dye adopts more standing-up orientation, with the average / standard deviation of distance between KU and cluster centers of mass of 1.49 / 0.05 nm. Also the dynamical behavior of the dyes at the two different pH conditions differ: principal components analysis reveal dye movements of compressing towards the structure, and flagging like motions for the fully protonated and fully deprotonated clusters, respectively.

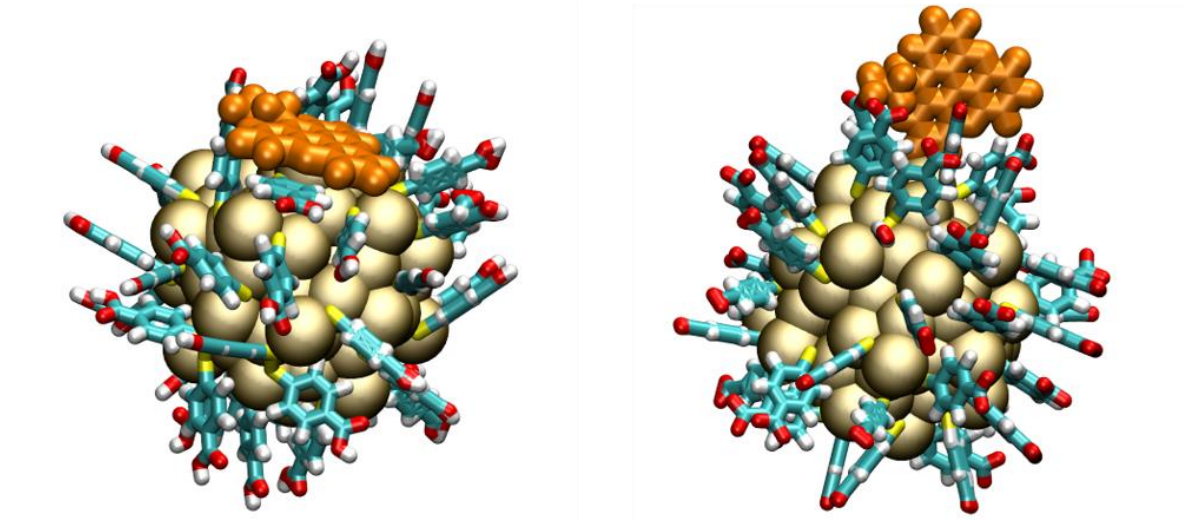

Figure SI5.2. A representative average structures from MD simulations of the fully protonated (left) and fully deprotonated (right) Au_{102} with covalently linked KU-dye.

SI6 Förster energy transfer

In this section, we consider the KU-Au_{102} complex from the point of view of energy transfer and associated quenching of fluorescence. Au_{102} possesses strong absorption throughout the visible spectral region making it a good acceptor of energy.[2]As the Au_{102} cluster is non-plasmonic and small, Förster theory for energy transfer should be a reasonable model for description of our system. Förster theory has been shown to work extremely well and it allows the calculation of energy transfer rates from spectroscopic experimental data.[3,4] We estimated the energy transfer rate constant k_{ET} for Förster resonance energy transfer theory [5] using the formula:

$$k_{ET} = k_D \left[\frac{R_0}{R}\right]^6 = \frac{1}{\tau_D^0}\left[\frac{R_0}{R}\right]^6 \qquad \text{(S1)}$$

where $k_D = 1/\tau_D^0$ is the decay rate of the donor (D) in the absence of the acceptor (A), and R is the distance between D and A. The Förster radius R_0 (ie. R when $k_{ET} = k_D$) is given by using

$$R_0^6 = \frac{9(ln10)}{128\pi^5 N_A}\frac{\kappa^2 \Phi_D}{n^4} J \qquad \text{(S2)}$$

, where J is the spectral overlap integral, κ^2 is the dipole orientation factor, n is the refractive index of the medium, and Φ_D is the quantum yield of the donor decay in the absence of the A. With known constants equation (2) can be expressed conveniently as

$$R_0 = 0.02108 \times \frac{\kappa^2 \Phi_D}{n^4} J\ . \qquad \text{(S3)}$$

The overlap integral

$$J = \int_0^\infty \tilde{I}_D\, \varepsilon_A(\lambda)\lambda^4 d\lambda \qquad \text{(S4)}$$

requires knowledge of the acceptor molar absorption coefficient $\varepsilon_A(\lambda)$ and the shape of the D fluorescence spectrum, which is normalized to unit area ($\int_0^\infty \tilde{I}_D\ d\lambda = 1$). For evaluation of J we used $\varepsilon_A(\lambda)$ values obtained from our previous work [1], and for $\tilde{I}_D$ KU emission spectrum measured in water at pH = 10.5 with λ = 500 nm excitation (Fig SI5.1).

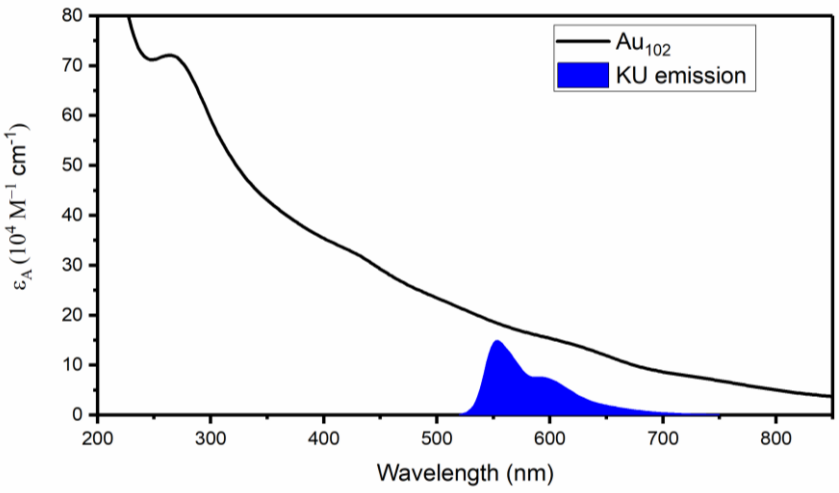

Figure SI6.1. Molar absorption coefficient of Au_{102} vs. KU emission spectrum used in the energy transfer simulations.

We numerically evaluated the integral $J = 1.88 \times 10^{16} M^{-1} cm^{-1} nm^4$. We assumed isotropic orientation $\kappa^2 = 2/3$ for the coupling dipoles. Basis for the assumption is to assume that Au_{102} electronic state density acts as an isotropic acceptor. In the simulation, refractive index of water n = 1.33 and Φ_D = 0.56 were used. We estimated Φ_D in water using a measured fluorescence life-time $\tau_F = 19ns$ in this work (SI9) in comparison with reported values for KU in acetonitrile $\Phi_D = 0.69$ and $\tau_F = 23ns$. [6] We obtained Förster radius using the equation (3), using R_0 = 7.6 nm. Calculated rate constants k_{ET} as a function of D-A distance are shown in Fig. SI5.2. In the figure, the approximate distance for the low pH and high pH configurations taken from the MD simulations (R = 1.3 nm) is marked.

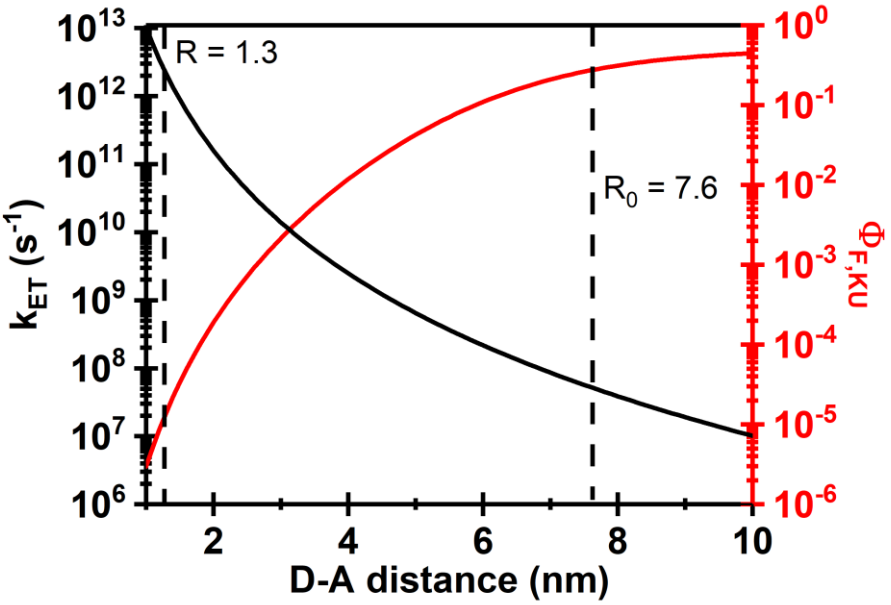

Figure SI6.2. Energy transfer rate constant k_{ET} and fluorescence quantum yield $\Phi_{F,KU}$ according to Förster theory for different Au_{102} (A)-Ku (D) distances.

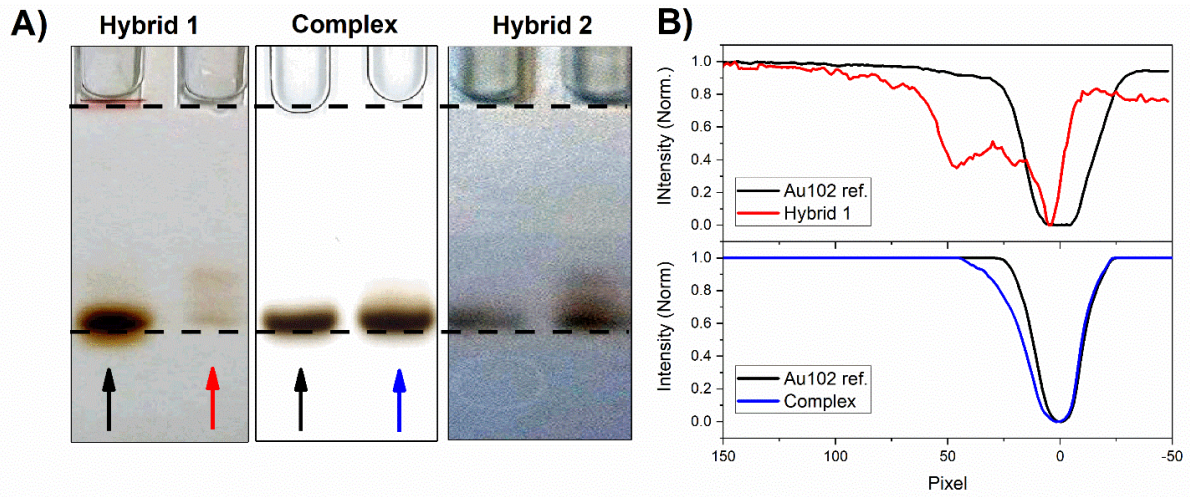

Figure SI7 A) Comparison of PAGE runs with Au_{102}-KU hybrid and Au_{102}-KU complex relative to Au_{102} references. To account the different PAGE running times the images have been scaled in way that bottom of the PAGE loading wells and the Au_{102} references have equal distances in the images (Black dashed lines). Presented Hybrid 1 and Hybrid 2 are from two different synthetic batches of hybrids. The complex has Au_{102}:KU ratio of 1:1. The image contrast in Hybrid 2 has been artificially increased for better comparison with other PAGE runs. (B) Normalized intensity cross-sections of Hybrid 1 and Complex PAGE images. The intensity cross-sections have been analyzed in the positions and in the direction indicated with color coded arrows in panel A). (Black arrows) Au_{102} references (Red arrow) Au_{102}-KU hybrid (Blue arrow) Au_{102}-KU complex. For the image intensity cross-section analysis, the original PAGE images have been converted to grayscale images. The background of individual cross-sections is normalized to 1 and the highest optical density position as 0. The pixel position of the intensity minima of Au_{102} references is set as 0.

SI8 Transmission electron microscopy images

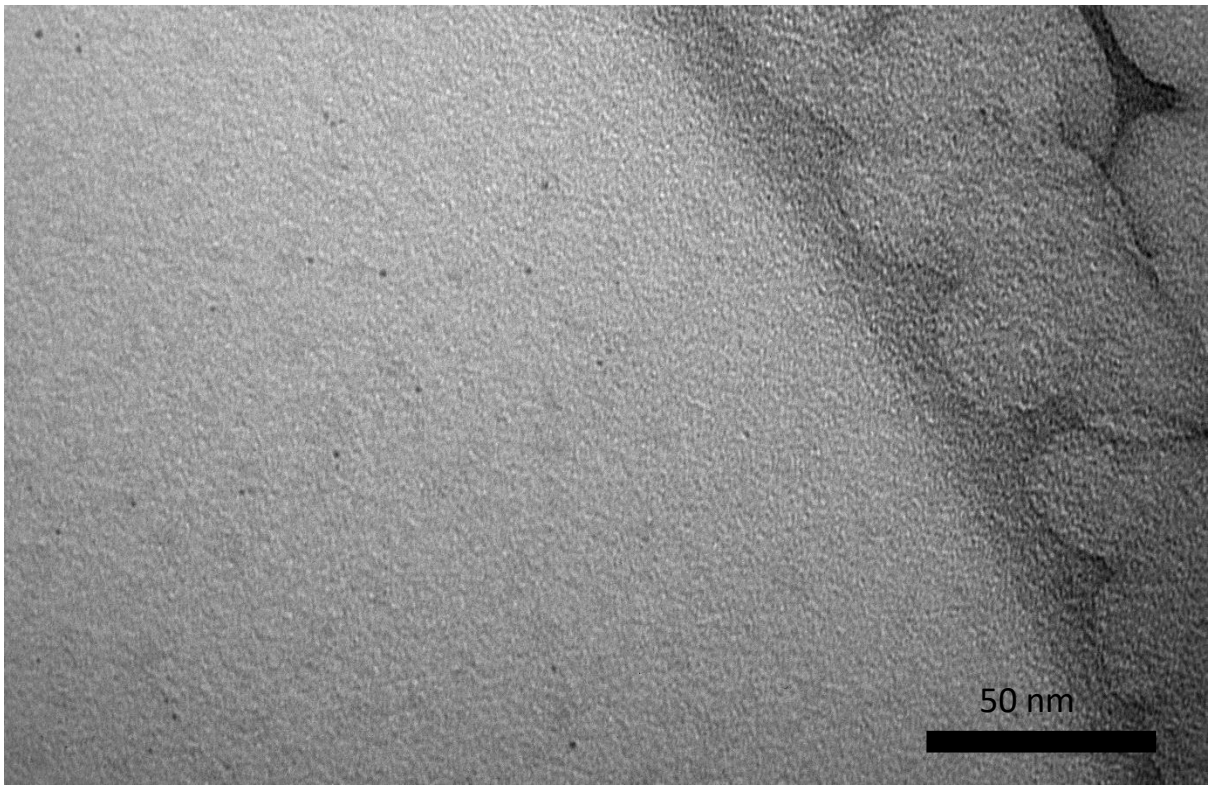

Figure SI8.1. TEM image of Au102-KU hybrid sample prepared at pH = 10

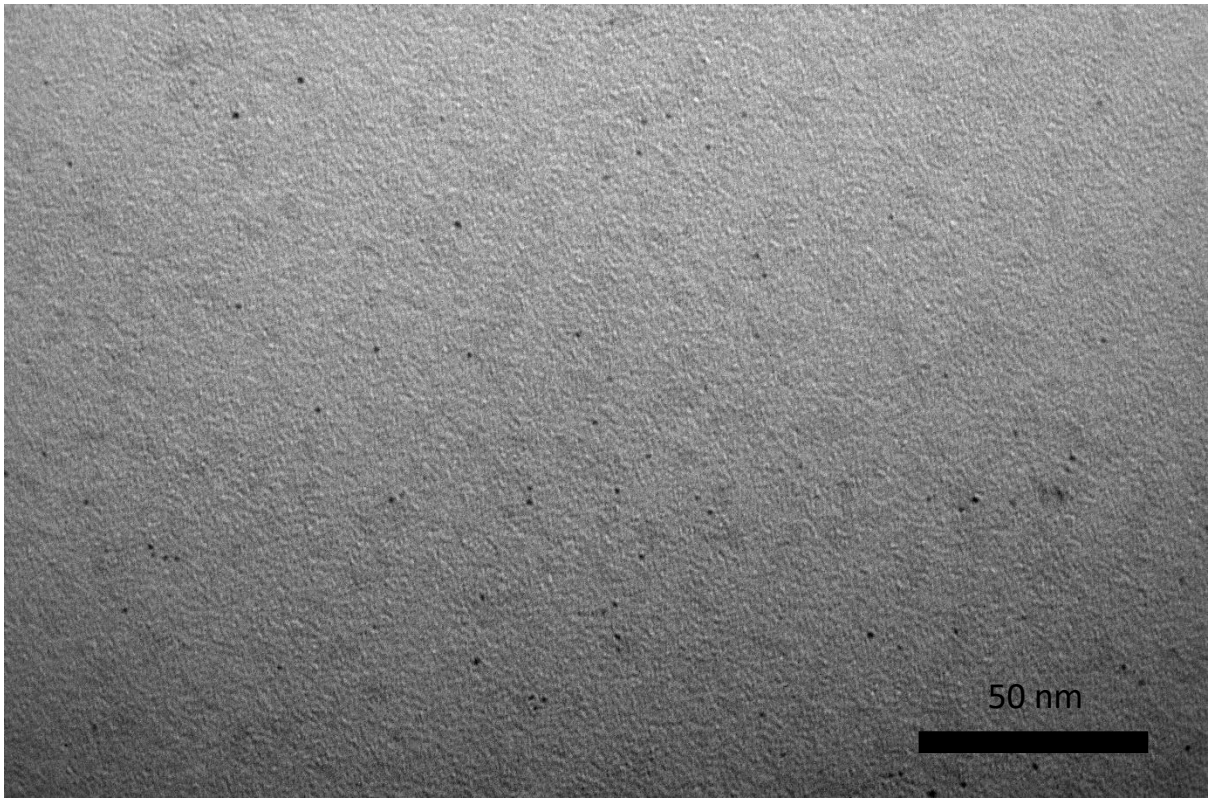

Figure SI8.2. TEM image of Au102-KU hybrid sample prepared at pH = 10

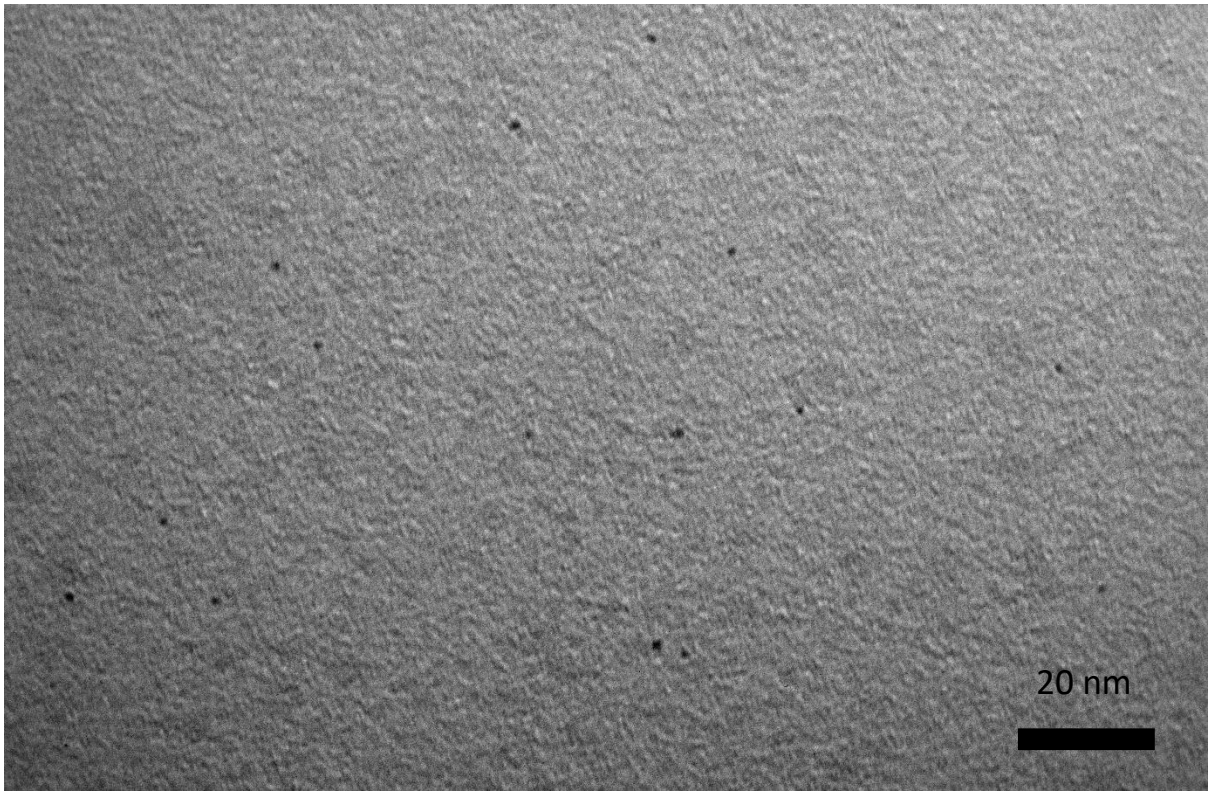

Figure SI8.3. TEM image of Au102-KU hybrid sample prepared at pH = 10

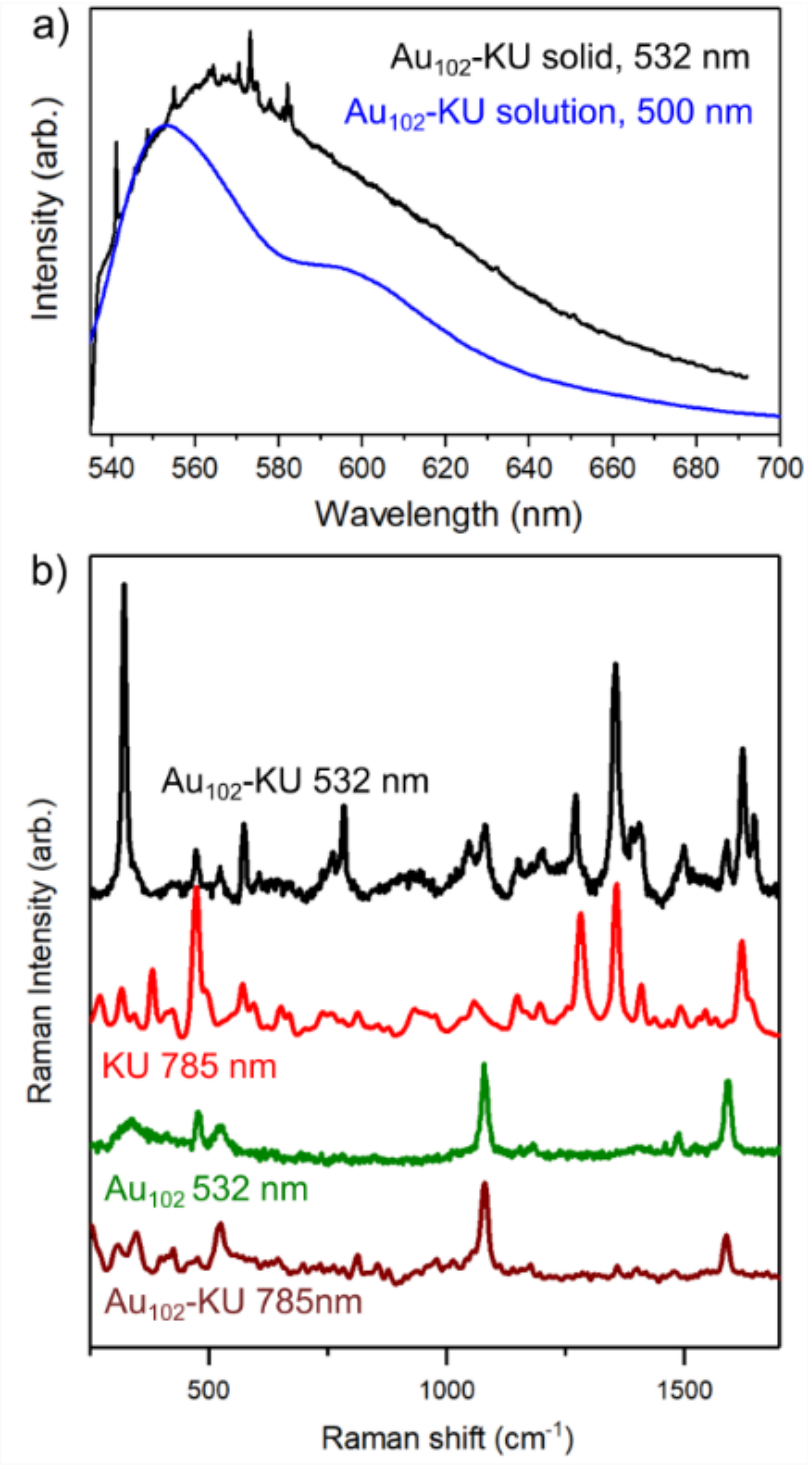

Fig. SI9. Raman spectra of Au_{102}-KU hybrid and its constituents. (a) Raman spectrum (excitation wavelength 532 nm) of Au_{102}-KU hybrid in solid form (black line) and fluorescence spectrum (excitation wavelength 500 nm) of Au-KU hybrid sample in solution. Raman spectrum shows clearly both broad fluorescence and narrow Raman peaks. (b) Raman spectra of Au_{102}-KU and bare KU excited at different wavelengths. Excitation of Au_{102}-KU with 532 nm (black line) shows strong resonance Raman spectrum of KU and Raman peaks of Au_{102}. Fluorescence signal subtracted. Non-resonant Raman spectrum of bare KU excited with 785 nm (red line) shows Raman peaks of KU. Raman spectrum of Au_{102}, excited with 532 nm (green line). Raman spectrum of Au_{102}-KU excited with 785 nm is not resonant with Ku and, thus only peaks of Au_{102} are visible.

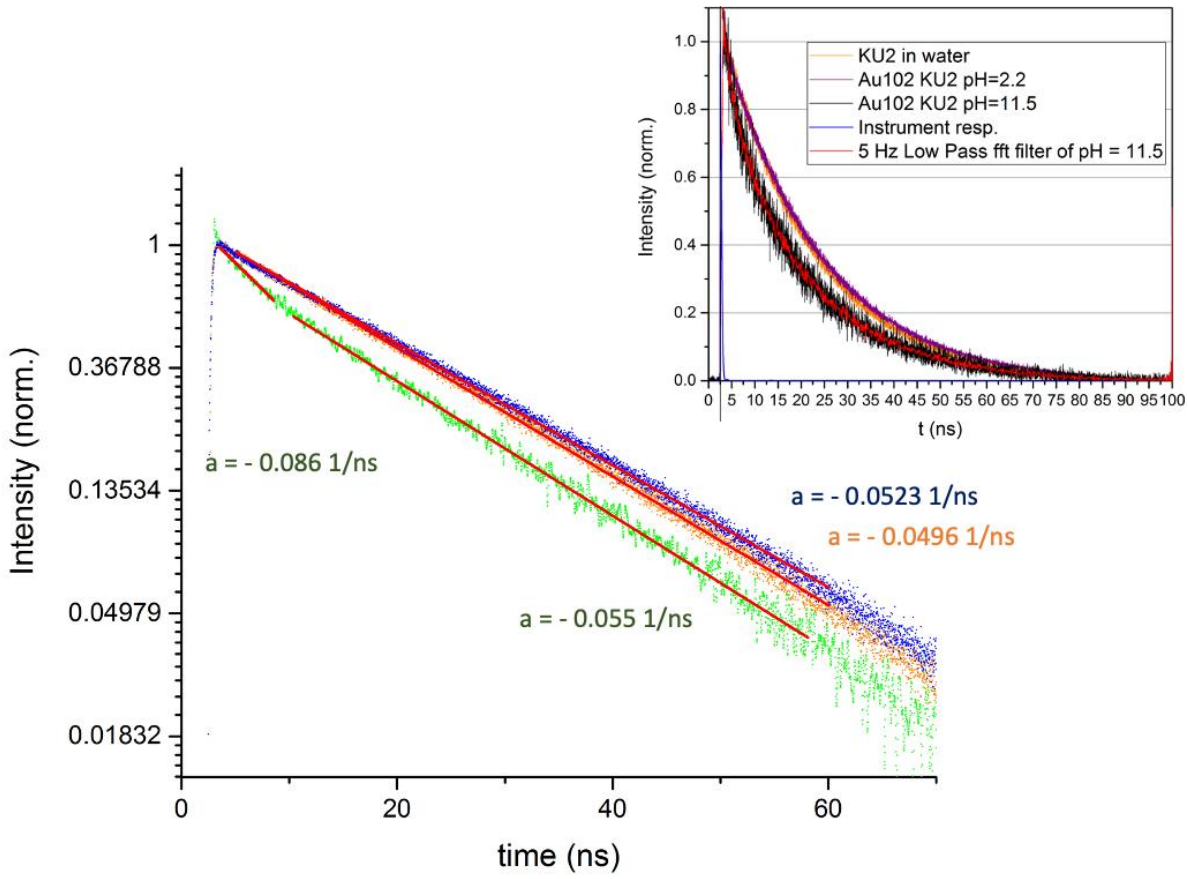

Fig SI10. (Inset) Normalized life-time decays of free aqueous KU-dye solution (yellow), Au_{102}-KU hybrid at pH = 2.2 (violet) and pH = 11.5 (black). Instrument response produced by the scattered ~100 ps laser pulse is shown with blue. The result of 5 Hz low-pass FFT noise-reduction filtering of the pH = 11.5 sample is shown with red. (Main panel) Life-time decays presented in ln-scale. (yellow points) aqueous KU-dye solution, Au_{102}-KU hybrid (blue points) pH = 2.2, (green points) pH = 11.5. (Red curves) Least-square linear fits ($y = ax + b$) to the data points. The negative slopes are the inverse of negative life-time. Fit parameters of the slope (a) are presented with color coded values. Note, the green points have been fitted with two linear functions for different life-time regions.

SI11. Lifetime measurement analysis. Time data was analyzed by standard fitting of the deconvolution of measured signal using two exponential function, with the instrument response IRF function.

$$f'(t) = f(t) \otimes IRF(t) = \int_{-\infty}^{\infty} f(T-t) IRF(T) dT \quad \text{(S5)}$$

Where,

$$f(t) = Ae^{-(t-t_0)/\tau_1} + Be^{-(t-t_0)/\tau_2} + C. \quad \text{(S6)}$$

In the expression t_0 is the zero-time, and C is amplitude at the infinite time (baseline). For IRF(t) we used Gauss function with FWHM ~ 100 ns.

SI12. Data analysis and processing of the microscopic data For measuring the intensities of the Au_{102}-KU conjugate in vesicles, multi-step segmentation implemented in the BioImageXD software[7] was used to isolate single structures from fluorescent data using the following protocol: at first stage the raw data were Gaussian smoothed using kernel size 1.0 to eliminate excess noise. Then the data were thresholded using intensity thresholding. The intensity threshold was selected experimentally so that the background fluorescence was kept very low. Objects were defined from the background using the connected component labeling tool embedded in the software. Average intensity of the objects was normalized to average area of the object or number of vesicles to produce sum of intensities. A t test was used for pairwise statistical comparison between samples.

Table SI12.1 Quantification of the probe intensity in vesicles before and after bafilomycin A1 treatment. After a 10 pulse of the probe or just dye (control) and chase until 2 h post internalisation (p.i.) cells were imaged by confocal microscopy and segmented for vesicle intensity quantification. Sum of intensities were calculated using similar thresholding for images with or without Bafilomycin A1. (**p <0.01 using t-test). Thresholds were however different between the probe and control in order to gain enough signal for the control case.

Sample	**probe intensity**
probe 2 h p.i.	101 +/- 1.9
probe + Baf A1	38 +/- 12.9** p=0.0032
Control	59.1 +/- 14.3
Control+ Baf A1	59.3 +/- 11.8 p=0.99

References

1. E. Thyrhaug, T. J. Sørensen, I. Gryczynski, Z. Gryczynski and B. W. Laursen, *Polarization and symmetry of electronic transitions in long fluorescence lifetime triangulenium dyes. J. Phys. Chem. A* 2013, **117**, 2160-2168.

2. E. Hulkko, O. Lopez-Acevedo, J. Koivisto, Y. Levi-Kalisman, R. D. Kornberg, M. Pettersson and H. Häkkinen, *Electronic and Vibrational Signatures of the Au_{102}(p-MBA)$_{44}$ Cluster, J. Am. Chem. Soc*. 2011, **133**, 3752 – 3755.

3. G. D. Scholes, *Long-Range Resonance Energy Transfer in Molecular Systems, Annu. Rev. Phys. Chem*., 2003, **54**, 57 – 87.

4. B. R. Masters, *Paths to Förster's Resonance Energy Transfer (FRET), Theory. Eur. Phys. J. H* 2014, **39**, 87–139.

5. Silvia E. Braslavsky, Eduard Fron, Hernán B. Rodríguez, Enrique San Román, Gregory D. Scholes, Gerd Schweitzer, Bernard Valeur and Jakob Wirz, *Pitfalls and limitations in the practical use of Förster's theory of resonance energy transfer, Photochem. Photobiol. Sci.*, 2008,**7**, 1444–1448.

6. S. A. Bogh, M. Simmermacher, M. Westberg, M. Bregnhøj, M. Rosenberg, L. De Vico, M. Veiga, B. W. Laursen, P. R. Ogilby, S. P. A. Sauer and T. J. Sørensen, *Azadioxatriangulenium and Diazaoxatriangulenium: Quantum Yields and Fundamental Photophysical Properties. ACS Omega*, 2017, **2**, 193 – 203.

7. P. Kankaanpää et al. *BioImageXD - an open general purpose and high throughput image processing and analysis platform for biomedical images. Nat. Methods.* 2012, **9**, 683-689.